Science Advances

AAAS

advances.sciencemag.org/cgi/content/full/3/1/e1601978/DC1

Supplementary Materials for

Electrospun core-shell microfiber separator with thermal-triggered flame-retardant properties for lithium-ion batteries

Kai Liu, Wei Liu, Yongcai Qiu, Biao Kong, Yongming Sun, Zheng Chen, Denys Zhuo, Dingchang Lin, Yi Cui

Published 13 January 2017, *Sci. Adv.* **3**, e1601978 (2017)
DOI: 10.1126/sciadv.1601978

The PDF file includes:

Other Supplementary Material for this manuscript includes the following:
(available at advances.sciencemag.org/cgi/content/full/3/1/e1601978/DC1)

- movie S1 (.mp4 format). The combustion of the EC/DEC electrolyte.
- movie S2 (.mp4 format). The combustion of the EC/DEC electrolyte with 40 wt % TPP.
- movie S3 (.mp4 format). The combustion of the TPP@PVDF-HFP separator wetted by the EC/DEC electrolyte.

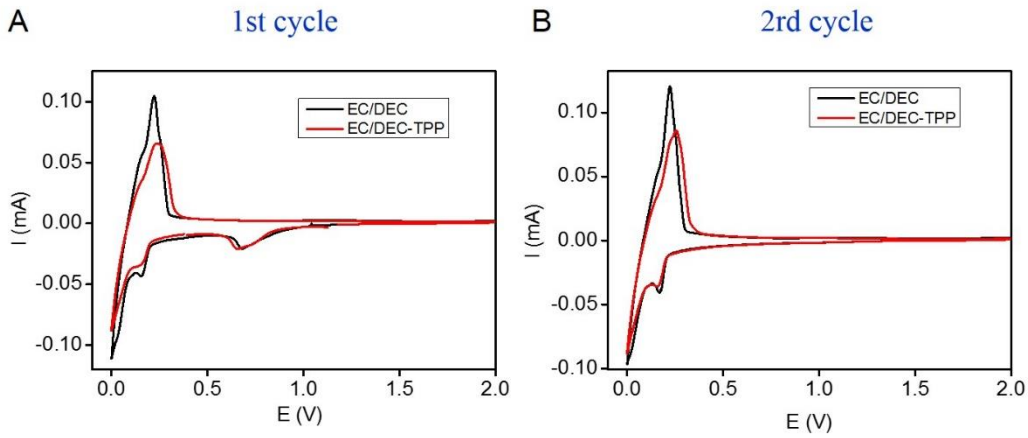

fig. S1. Cyclic voltammogram for the graphite anode in different electrolytes. The CV were scanned from 2.0 V to 0.01 V versus Li/Li^+ at a 0.05 mV/s scan rate. (**A**) The first cycle, (**B**) the second cycle.

In cyclic voltammetry (CV) measurements (fig. S1), no new redox peaks were detected in the presence of TPP compared with the pristine electrolytes, indicating that TPP did not interfere with the electrochemical reactions on the graphite anodes.

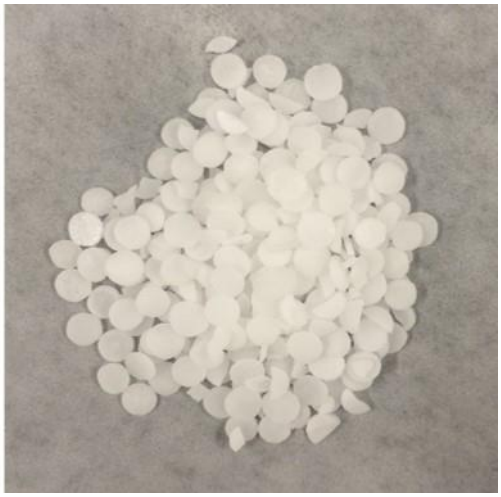

fig. S2. A digital photograph showing that the TPP molecules are flake-like crystals.

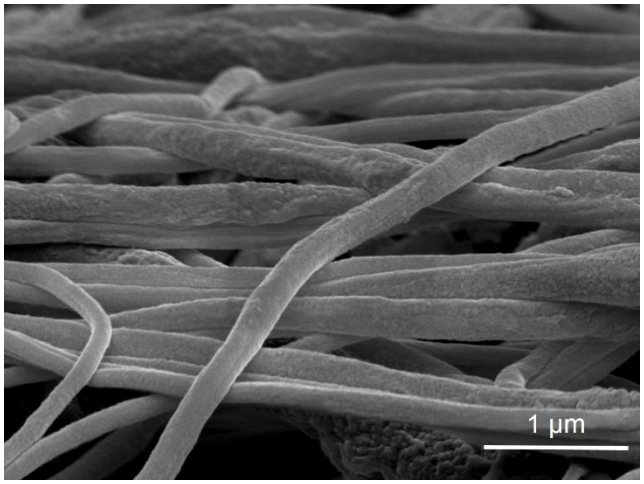

fig. S3. SEM image of the TPP@PVDF-HFP fibers.

Discussion on the thickness of the PVDF-HFP shell and the diameter for the individual fibers: The average diameter of the TPP@PVDFHFP fibers is ~900 nm. We tried TPP@PVDFHFP fibers with other different diameters by tuning the parameters of electrospinning (viscosity of the feeding solution, electrospinning voltage). We find that the performance of the TPP@PVDF-HFP separator is not sensitive to the diameter of its individual fibers. For fibers with smaller diameters (for example, ~200 nm, as shown in fig. S3), the separator still functions well. However, it is hard to get fibers with a diameter larger than 900 nm using electrospinning. The major issue during attempts to get thicker fiber is that the viscosity of the feeding solution is too high for continuous spinning during our attempts to get fibers with bigger diameters.

As for the diameter for the PVDF-HFP shell, it is determined by the weight ratio of PVDF-HFP and TPP in the fiber. In our study, the weight ratio of PVDF-HFP and TPP is designed considering that if all the TPP in the fiber is released into the electrolyte, the final concentration of TPP (~30 wt%) in the electrolyte is high enough for retarding the flame. If the weight ratio of PVDF-HFP:TPP increases, the thickness of the shell will increase and the separator is not efficient in carrying enough TPP to retard the flame. On the other hand, if the weight ratio of PVDF-HFP:TPP decreases, the thickness of the shell will decrease and will not be efficient in encapsulating TPP inside the shell.

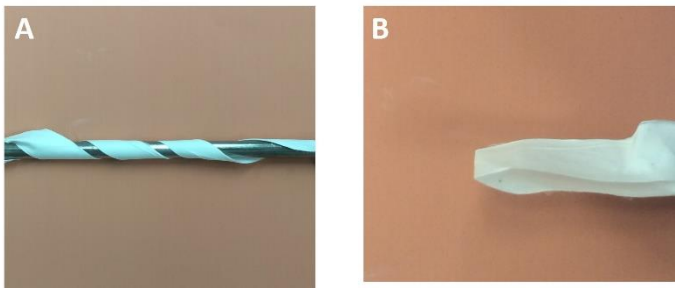

fig. S4. Digital pictures showing the (A) flexibility and (B) bendability of the TPP@PVDF-HFP membranes.

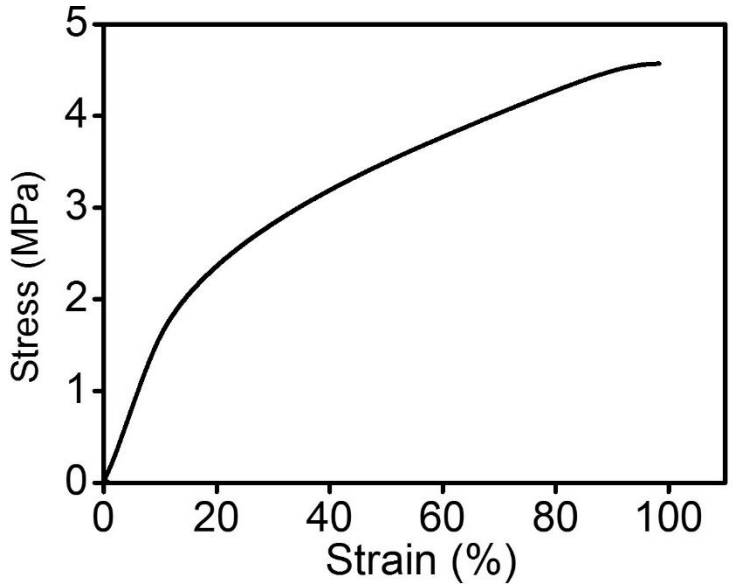

fig. S5. The stress-strain curve of the TPP@PVDF-HFP membrane.

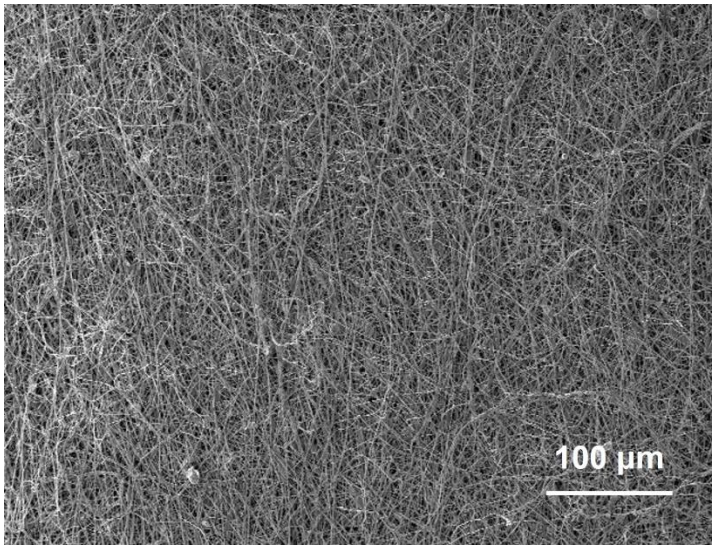

fig. S6. SEM image of the TPP@PVDF-HFP membrane.

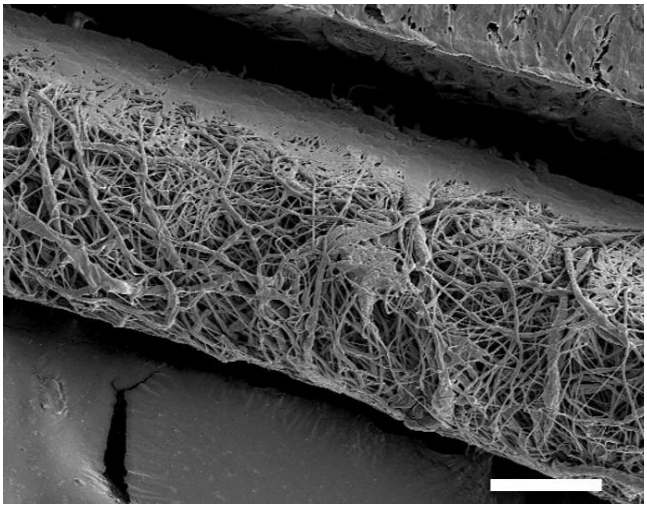

fig. S7. SEM cross-sectional image of the TPP@PVDF-HFP separator. Scale bar, 20 µm.

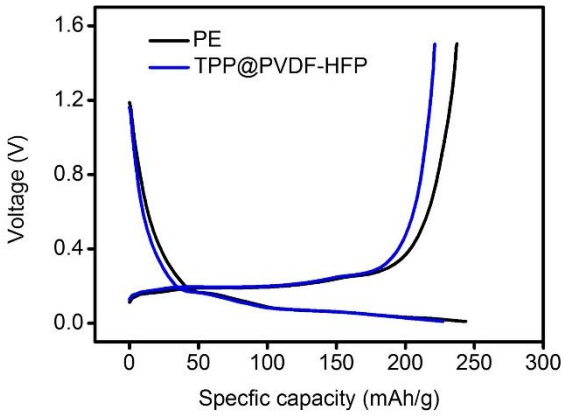

fig. S8. Voltage profiles of the graphite anode using the PE (black curve) separator and the TPP@PVDF-HFP separator (blue curve). The charge/discharge rate is 1C.

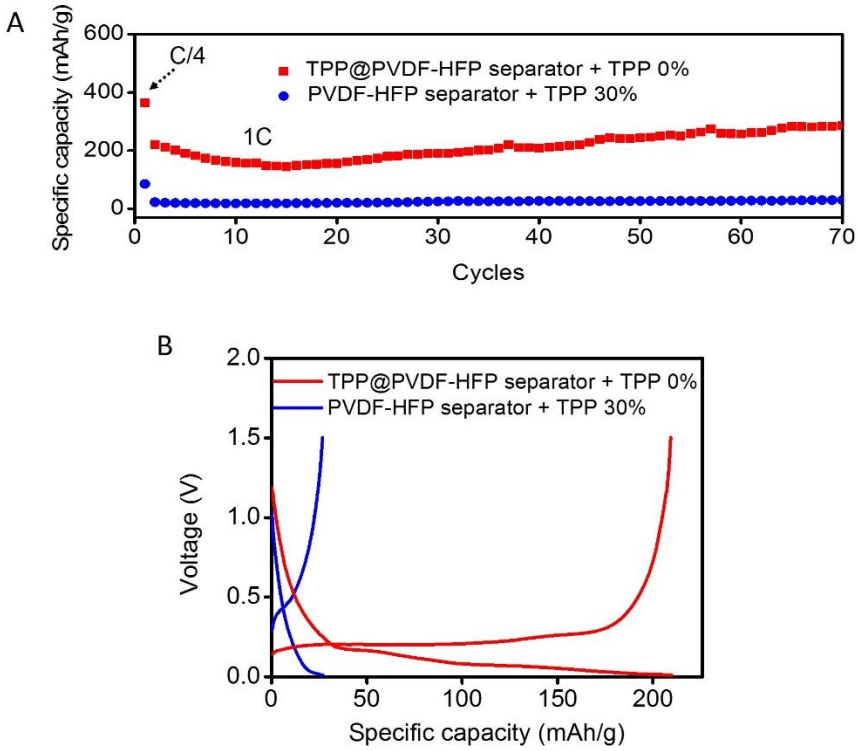

fig. S9. Electrochemical performances of the graphite anode using TPP@PVDF-HFP separators and PE separators with different electrolytes. (**A**) Delithiation capacities of the graphite anode during galvanostatic cycling between 0.01−1.5V. The rate was 0.25 C for the first cycle, and 1C for the later cycles. (**B**) Galvanostatic charge/discharge voltage profiles for the graphite anode plotted for the 40th cycle. Different combinations of electrolytes and separators were used in (A) and (B). Red color: TPP@PVDF-HFP separator + Pristine EC/DEC electrolyte; Blue color: PVDF-HFP separator + EC/DEC electrolyte containing 30 wt% TPP.

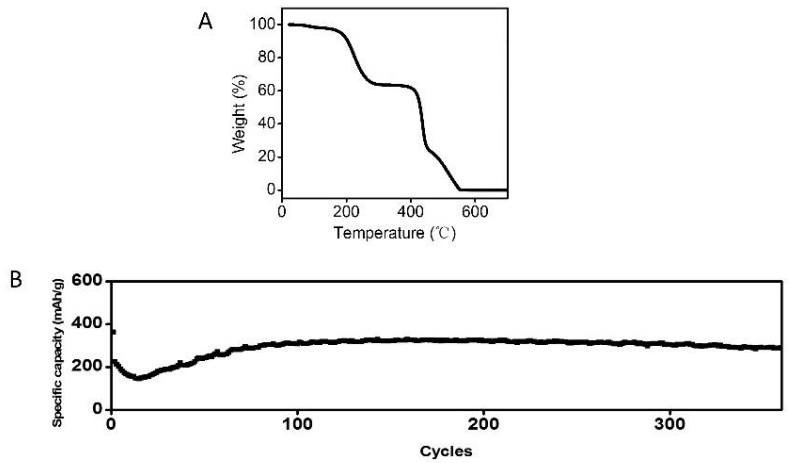

fig. S10. TGA measurements of the TPP@PVDF-HFP separator after long term cycling and the electrochemical performance of related battery. (**A**) TGA measurements of the fibers after long electrochemical cycling. (**B**) Long term delithiation capacities of the graphite anode during galvanostatic cycling between 0.01−1.5V. The rate was 0.25 C for the first cycle, and 1C for the later cycles.

Discussion on the swelling of PVDF-HFP shell by the electrolyte:

It should be noted that during long term cycling, the PVDF-HFP shell can absorb the electrolyte and swell a little bit, due to which a small amount of TPP will gradually diffuse out the fibers and dissolve into the electrolyte. The swelling ratio of the separator in the presence of standard EC/DEC was measured to be 15%, which is quite small (see Materials and Methods in the main text). Even considering that TPP will contact with EC/DEC that has penetrated into the fiber, the diffusion across the polymer barrier shells should be quite slow.

To test the long-term stability of the TPP@PVDF-HFP separator, we measured the TPP content remaining in the fiber after long-term cycling (360 cycles). As can be seen from the TGA curve in fig. S10A, about 15% of the original TPP was lost, then the concentration of TPP in the EC/DEC electrolyte was then be calculated to be ~4.5 wt%.

The low concentration of TPP in the EC/DEC electrolyte did not affect the battery performance too much, although the capacity is a little bit lower than the PE separator case as shown in Fig. 4A in the main text. Also, after long term cycling, the graphite anode still shows a high capacity at high charge/discharge rate (1C). As can be seen from the long term cycling stability curve in fig. S10B, the average specific capacity of the graphite anode for the first 360 cycles was measured to be 293 mAh/g at 1C charge/discharge rate.

To conclude, the swell of the PVDF-HFP shell by the EC/DEC electrolyte has not significantly affected the electrochemical performances of batteries.

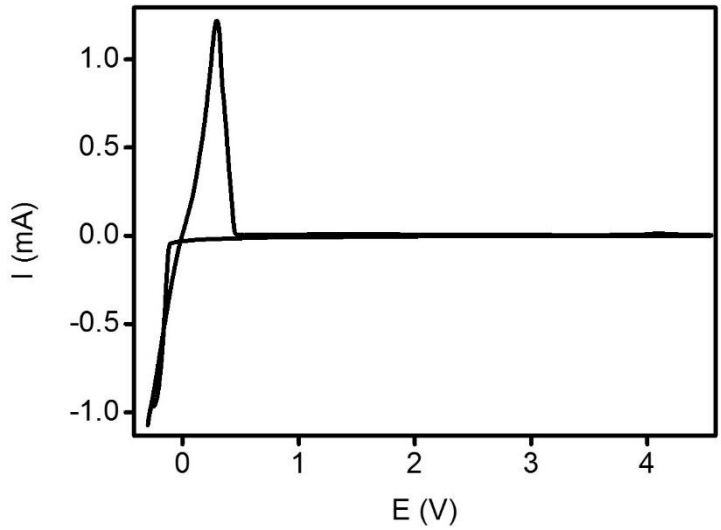

fig. S11. Electrochemical stability of the TPP@PVDF-HFP separator. The CV were scanned from -0.3 V to 4.5 V versus Li/Li^+ at a 0.5 mV/s scan rate. The peaks at -0.24 V and 0.29 V is attributed to the Li deposition and stripping process, respectively.

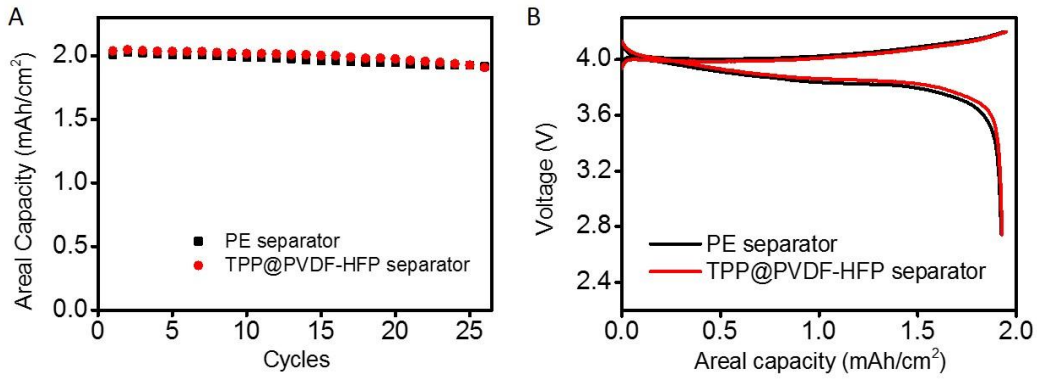

fig. S12. The electrochemical stability of the TPP@PVDF-HFP separator towards LCO cathode. (**A**) Cycling performance of the $LiCoO_2$ cathode during galvanostatic cycling between 2.75−4.2V. The current density is 1.5mA. Different separators were used. Black squares: PE separator. Red circles: TPP@PVDF-HFP separator. (**B**) Charge/discharge voltage profiles of the $LiCoO_2$ cathode with different separators. Black lines: PE separator. Red lines: TPP@PVDF-HFP separator.

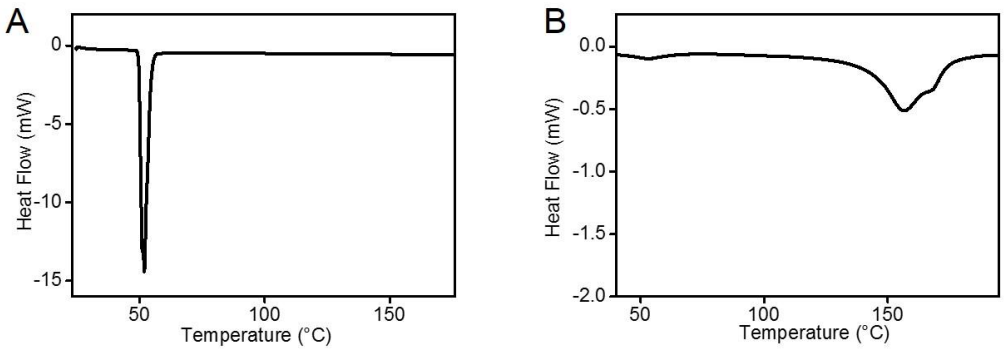

fig. S13. The measurements on the T_m of TPP and PVDF-HFP. DSC profiles of (A) TPP, and (B) PVDF-HFP, respectively.

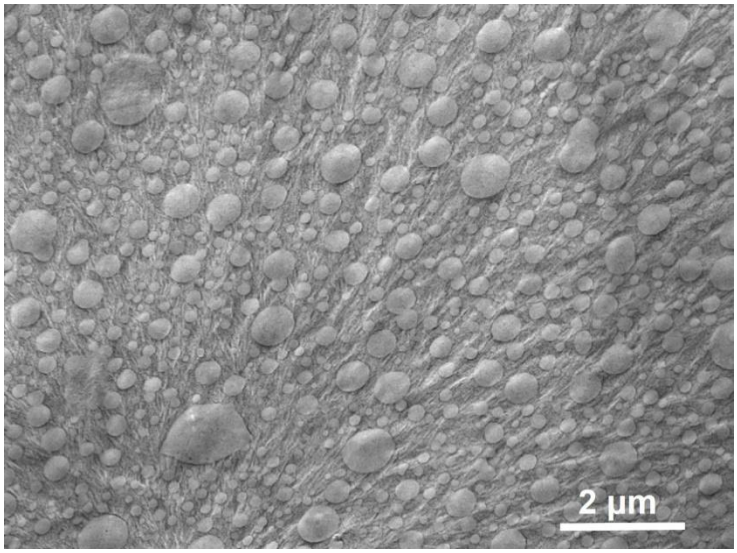

fig. S14. SEM image of the TPP@PVDF-HFP after heat treatment. To study the response of the TPP@PVDF-HFP microfibers upon thermal stimuli, the separator was heated to 160°C (above the melting point of PVDF-HFP), and cooled to room temperature. As shown in fig. S5, the microfibers melted, forming a bulk polymer material. The TPP flakes are clearly visible on the surface of the polymer, indicating that embedded TPP was released out after the polymer shell is melted.

movie S1. The combustion of the EC/DEC electrolyte.

movie S2. The combustion of the EC/DEC electrolyte with 40 wt % TPP.

movie S3. The combustion of the TPP@PVDF-HFP separator wetted by the EC/DEC electrolyte.